Coherent versus incoherent excitation energy transfer in molecular systems

Hung-Tzu Chang and Yuan-Chung Cheng

Citation: J. Chem. Phys. **137**, 165103 (2012); doi: 10.1063/1.4761929
View online: http://dx.doi.org/10.1063/1.4761929
View Table of Contents: http://jcp.aip.org/resource/1/JCPSA6/v137/i16
Published by the American Institute of Physics.

Coherent versus incoherent excitation energy transfer in molecular systems

Hung-Tzu Chang and Yuan-Chung Cheng[a)]
Department of Chemistry and Center for Quantum Science and Engineering, National Taiwan University, Taipei City 106, Taiwan

(Received 20 August 2012; accepted 8 October 2012; published online 25 October 2012)

We investigate the Markovian limit of a polaronic quantum master equation for coherent resonance energy transfer proposed recently by Jang *et al.* [J. Chem. Phys. **129**, 101104 (2008)]. An expression for the rate of excitation energy transfer (EET) is derived and shown to exhibit both coherent and incoherent contributions. We then apply this theory to calculated EET rates for model dimer systems, and demonstrate that the small-polaron approach predicts a variety of dynamical behaviors. Notably, the results indicate that the EET dynamical behaviors can be understood by the interplay between noise-assisted EET and dynamical localization, while both are well captured by the polaron theory. Finally, we investigate bath correlation effects on the rate of EET and show that bath correlations (or anti-correlations) can either enhance or suppress EET rate depending on the strength of individual system-bath couplings. In summary, we introduce the small-polaron approach as an intuitive physical framework to consolidate our understanding of EET dynamics in the condensed phase.
 [http://dx.doi.org/10.1063/1.4761929]

I. INTRODUCTION

Excitation energy transfer (EET) processes have attracted intensive research interests in chemistry and physics because of their fundamental importance in phenomena such as photosynthesis, photocatalytic chemistry, and operation of optoelectronic devices.[1] For example, natural photosynthesis utilizes sophisticated molecular apparatus in the form of compact pigment-protein complexes to perform solar energy harvesting and trapping in remarkably high efficiency.[2–4] Thus, understanding the mechanism of highly efficient excitation energy transduction among and within photosynthetic complexes could provide valuable insights for improving the design and performance of artificial solar energy harvesting devices.

Despite intensive research, recent experiments based on ultrafast spectroscopic techniques have shown that conventional theoretical frameworks cannot adequately describe EET processes in photosynthesis and many organic materials.[5–10] Moreover, theoretical analyses based on nonperturbative hierarchical equation of motion approaches[11–14] have shown that non-Markovian dynamics, coherence dynamics, and multi-phonon effects are important in ultrafast EET processes. Although numerically exact nonperturbative approaches capture these effects and have been successfully applied to provide useful insights into the dynamics of light harvesting,[14–16] they are computationally intensive and often require special numerical implementations and even high-performance hardware in order to treat realistic models for photosynthetic systems.[17] For example, Kreisbeck and Kramer[14] have recently calculated the two-dimensional electronic spectra of a medium-size (with 7 chromophores) photosynthetic complex with realistic spectral density using a hierarchical equation of motion approach implemented on graphics processing units. Therefore, the development of a generalized theory that is applicable to coherent EET in large molecular systems (with >100 chromophores in a normal antenna supercomplex) in a broad parameter range is still highly desirable.

Recently, a small-polaron quantum master equation (SP-QME) has been developed by Jang *et al.* and independently by Nazir and co-workers to treat coherent evolutions and non-Markovian dynamics in EET processes.[18–23] This approach adopts a fundamentally different picture for EET by using a combined electronic/vibrational basis called "small polaron states" to describe EET dynamics, assuming that the electronic excitation moves collectively with its surrounding bath deformation instead of treating the electronic and vibrational degrees of freedom separately. The small-polaron approach has been successfully applied to describe EET in the intermediate coupling regime,[18,23] in which the strengths of electronic coupling and electron-phonon coupling are comparable. While more recently it has been shown that various variational polaron approaches yield superior results,[24–28] the small-polaron approach still provides a simple perturbative approach that gives adequate results over a broad parameter range.[23,27]

To further our understanding of EET in condensed-phase molecular systems and to elucidate the interplay between coherent and incoherent EET mechanisms, we investigate EET rate in the Markovian limit of the SP-QME theory in this work. We aim to shed light on the mechanisms that contribute to the non-trivial temperature and coupling-strength dependences of EET dynamics by considering the polaronic representation of EET dynamics. This paper is organized as follows. In Sec. II we outline the Markovian SP-QME theory and

a)Electronic mail: yuanchung@ntu.edu.tw.

the model system studied in this paper. Critical to the theory is the small-polaron transformation that leads to a renormalized Hamiltonian with a small interaction term at both the strong electronic coupling and the strong electron-phonon coupling limits. Additionally, we adopt as the model system a dimer system with a general bath model that treats bath correlations. For the dimer model, we demonstrate that the Markovian EET rate given by the small-polaron theory contains both coherent and incoherent contributions. In Sec. III we present the main results of this work and discuss their implications. We first investigate dynamical localization in the small-polaron picture and its effects on the EET dynamics and equilibrium structures of excitonic systems. Then, by calculating EET rates for the model dimer system at various temperatures and system-bath coupling strengths, the behaviors of EET dynamics are explored in a broad parameter range. In addition, we study the effects of bath correlations on the EET rates. The results indicate that the small-polaron approach not only predicts a wealth of different EET dynamical behaviors but also offers a intuitive physical framework to describe EET dynamics in the condensed phase. Finally, we summarize and discuss the main results of this work in Sec. IV.

II. THEORY

A. Polaron transformation

To describe EET in a multichromophoric system, we consider a model with N chromophores coupled to a harmonic bath through bilinear exciton-phonon couplings in the following system-plus-bath Hamiltonian ($\hbar = 1$):[4,29]

$$\begin{aligned} H &= H_s + H_b + H_{sb}, \\ H_s &= \sum_{i=1}^{N} \mathcal{E}_i a_i^\dagger a_i + \sum_{i\neq j} J_{ij} a_i^\dagger a_j, \\ H_b &= \sum_n \omega_n \left(b_n^\dagger b_n + 1/2\right), \\ H_{sb} &= \sum_{i,n} \omega_n g_{ni} a_i^\dagger a_i \left(b_n + b_n^\dagger\right), \end{aligned} \tag{1}$$

where H_s denotes the Frenkel-exciton Hamiltonian of the system, in which $a_i^\dagger$ is the exciton creation operator for an excitation on the ith chromophore (site), $\mathcal{E}_i$ is the optical transition energy of the ith site, and J_{ij} denotes the electronic coupling between the ith and jth site. H_b describes the phonon bath, and $b_n^\dagger$ is the creation operator of the nth phonon mode. H_{sb} describes the exciton-phonon (or system-bath) couplings, in which g_{ni} is the unitless exciton-phonon coupling constant between the ith site and the nth phonon mode. Note that in the Hamiltonian we do not assume independent bath modes for each site, therefore, the general situations of correlated baths can be treated in this model.

Polaron theories have long been used to treat exciton- and electron-phonon interactions in solids. The "small polaron" formalism, pioneered by Holstein to treat charge transfer in organic molecular crystals,[30] is later extended by Silbey and co-workers to treat population dynamics in EET.[24,31] To reach a renormalized Hamiltonian that contains small interaction terms at both the strong electronic coupling ($J \gg 1$) and strong electron-phonon coupling limits ($g \gg 1$), we follow Grover and Silbey[31] and define a unitary transformation (the so-called small-polaron transform) using $U = e^S$, where $S = -\sum_{i,n} g_{ni} a_i^\dagger a_i (b_n - b_n^\dagger)$. Applying the transformation to the Hamiltonian and rearranging the terms lead to a renormalized Hamiltonian,[18,31]

$$\begin{aligned} \tilde{H} &= U^\dagger H U = \tilde{H}_s + \tilde{H}_{sb} + \tilde{H}_b, \\ \tilde{H}_s &= \sum_{i=1}^{N} (\mathcal{E}_i - \lambda_i) a_i^\dagger a_i + \sum_{i\neq j} J_{ij} \langle \theta_i^\dagger \theta_j \rangle a_i^\dagger a_j, \\ \tilde{H}_b &= H_b, \\ \tilde{H}_{sb} &= \sum_{i\neq j} J_{ij} (\theta_i^\dagger \theta_j - \langle \theta_i^\dagger \theta_j \rangle), \end{aligned} \tag{2}$$

where λ_i is the reorganization energy for the ith site, $\lambda_i = \sum_n g_{ni}^2 \omega_n$, and θ is a phonon displacement operator defined by

$$\theta_i = \exp\left[\sum_n g_{ni} \left(b_n - b_n^\dagger\right)\right].$$

The unitary transformation effectively changes the basis to a small-polaron basis that contains excitons and their associated displaced phonon modes. In the small-polaron basis, reorganization energy terms are added to the diagonal site energies, and the electronic couplings are renormalized by a factor $\langle \theta_i^\dagger \theta_j \rangle$. Here, we define effective electronic couplings by

$$\tilde{J}_{ij} = J_{ij} \langle \theta_i^\dagger \theta_j \rangle, \tag{3}$$

where the thermal average in the renormalization factor can be evaluated to give

$$\langle \theta_i^\dagger \theta_j \rangle = \exp\left[-\frac{1}{2} \sum_n (g_{ni} - g_{nj})^2 \coth \frac{\beta \omega_n}{2}\right],$$

with inverse temperature $\beta = (k_B T)^{-1}$. The renormalization factor $\langle \theta_i^\dagger \theta_j \rangle$ is a thermal-averaged Franck-Condon factor that describes the overlap between two displaced phonon wavefunctions and depends on both temperature and exciton-phonon coupling strengths: it approaches zero at high temperatures or strong exciton-phonon couplings. The effective electronic coupling, $\tilde{J}_{ij}$, is directly influenced by the renormalization factor and the effects of which on the equilibrium structures and EET dynamics will be investigated in Sec. III A.

The renormalized system-bath coupling term, $\tilde{H}_{sb}$, describes the *fluctuations* of the phonon-modulated effective electronic couplings. This perturbation term is deliberately chosen such that the thermal average $\langle \tilde{H}_{sb} \rangle = 0$. The repartition is a distinct feature of this theory, which is different from many other approaches based on the same polaronic picture. For example, Kenkre and Knox's generalized master equation approach[32] adopted the full renormalized electronic couplings as the perturbation term.

Finally, we introduce spectral density $\mathfrak{J}(\omega)$ to treat system-bath couplings. The spectral density function is

defined as

$$\mathfrak{J}_{ij}(\omega) = \sum_n g_{ni} g_{nj} \omega_n^2 \delta(\omega - \omega_n), \tag{4}$$

where $\mathfrak{J}_{ii}$ describes diagonal exciton-phonon couplings to the ith site, and $\mathfrak{J}_{ij}$, when $i \neq j$, describes exciton-phonon couplings shared between the ith and jth sites. Therefore, cross-correlations between energy fluctuations on different sites can be treated in this formalism. Details on the evaluations of reorganization energies and thermal-averaged Franck-Condon factor in terms of spectral densities are given in Appendix A.

B. Markovian master equation and rate expression

The small-polaron transform has been applied to treat various electron-phonon coupled problems, but previous treatments almost universally consider only population dynamics.[24,30,31,33] Motivated by recent experiments showing quantum coherence effects in EET of photosynthetic complexes,[5,8,9] Jang *et al.* have recently derived a full small-polaron quantum master equation in which coherent evolutions and non-Markovian dynamics are explicitly included.[19] The SP-QME allows us to elucidate how quantum coherences between excitonic states affect the excitation energy transfer and how protein dynamics is coupled to the dynamics of electronic energy transfer between chromophores in photosynthetic complexes. For the completeness of this work, in the following we present the key results of this formalism and then focus on the population dynamics predictions by the SP-QME approach.

Following Zwanzig's projection operator technique[34] and using the renormalized $\tilde{H}_{sb}$ as the perturbation term, Jang *et al.* obtained the equation of motion for the reduced density matrix of the excitonic system,[20]

$$\begin{aligned}\dot{\sigma}(t) = &-i[\tilde{H}_s, \sigma(t)] \\ &- \int_0^t d\tau \mathrm{Tr}_b \left\{\left[\tilde{H}_{sb}(0), \left[\tilde{H}_{sb}(-\tau), \sigma(t) \otimes \rho_b^{eq}\right]\right]\right\} \\ &- i\mathrm{Tr}_b\left\{\left[\tilde{H}_{sb}(0), e^{-i(\tilde{H}_s+\tilde{H}_b)t}\left(\rho_T(0) - \sigma(0) \otimes \rho_b^{eq}\right)\right.\right. \\ &\left.\left. \times e^{i(\tilde{H}_s+\tilde{H}_b)t}\right]\right\} \\ &- \int_0^t d\tau \mathrm{Tr}_b\left\{\left[\tilde{H}_{sb}(0), \left[\tilde{H}_{sb}(\tau - t), e^{-i(\tilde{H}_s+\tilde{H}_b)t}\right.\right.\right. \\ &\left.\left.\left. \times \left(\rho_T(0) - \sigma(0) \otimes \rho_b^{eq}\right)e^{i(\tilde{H}_s+\tilde{H}_b)t}\right]\right]\right\},\end{aligned} \tag{5}$$

where $\mathrm{Tr_b}\{\}$ represents trace over bath degrees of freedom and ρ_b^{eq} is the bath equilibrium density matrix of H_b. The time evolution of an operator $A(\tau)$ is defined in the interaction picture of the zeroth Hamiltonian, $\tilde{H}_0 = \tilde{H}_s + \tilde{H}_b$. Equation (5) is valid for arbitrary initial conditions and multichromophoric systems,[19,20,23] in which the first term describes the coherent dynamics driven by the renormalized system Hamiltonian, the second term describes dissipative dynamics induced by the bath fluctuations, and the last two terms are inhomogeneous terms that capture the non-equilibrium dynamics during the bath reorganization processes.[19] The inhomogeneous terms decay to zero at times longer than the bath relaxation time and therefore do not contribute to the relaxation rate at the long-time limit.[35,36] Therefore, to focus on the EET dynamics we neglect the inhomogeneous terms and take the long-time limit of the memory kernel[37] to arrive at a Markovian form,

$$\begin{aligned}\dot{\sigma}(t) = &-i[\tilde{H}_s, \sigma(t)] \\ &- \int_0^\infty d\tau \mathrm{Tr_b}\left\{\left[\tilde{H}_{sb}, \left[\tilde{H}_{sb}(-\tau), \sigma(t) \otimes \rho_b^{eq}\right]\right]\right\}.\end{aligned} \tag{6}$$

This equation describes EET dynamics of a polaronic system induced by the fluctuations of effective electronic couplings. Here, the Markovian approximation is applied, therefore, Eq. (6) is valid when the EET dynamical time scale is longer than the bath relaxation time (i.e., fast bath).[27,36] Given that the bath-relaxation time in a typical photosynthetic system is usually <100 fs and that the majority of the population transfer time scale ranges from a few hundred femtoseconds to a few picoseconds in photosynthetic systems, the Markovian dynamics should capture a major portion of EET dynamics in photosynthetic light harvesting.[4]

In addition, the polaronic quantum master equation describes the EET dynamics in a displaced bath representation, which significantly reduces shortcomings of Markovian master equation and thus has a wider range of applicability compared to the conventional weak-coupling Redfield equation.[35] However, this change of basis also complicates the interpretation of the polaronic reduced density matrix $\sigma(t)$, because the total density matrix is dressed with bath displacements before traced over bath degrees of freedom,

$$\sigma_{ij} = \mathrm{Tr}_b\left\{\theta_i^\dagger \rho_{ij} \theta_j\right\}, \tag{7}$$

where ρ denotes the total system-plus-bath density matrix and $\rho_{ij} = \langle i|\rho|j\rangle$. Here, the diagonal elements of the reduced density matrix are invariant under the polaron transformation, however, the off-diagonal elements (coherences) are mingled with bath averages compared with the respective original site-basis coherences.[18,20] Therefore, in general it is non-trivial to recover coherences in the original undressed basis from $\sigma(t)$ in the polaronic representation. As a result, an observable that depends on the coherences in the undressed site basis would be difficult to evaluate from the polaronic reduced density matrix. For example, calculation of absorption spectrum is non-trivial in the polaronic representation.[18,20] Nevertheless, a limiting case can be considered: when the bath relaxation is rapid and thus an equilibrium bath can be presumed, the trace over the off-diagonal elements in Eq. (7) reduces to thermal averages. As a result, a coherence in the polaronic representation equals to the respective coherence in the undressed site basis multiplied by a Frank-Condon factor due to bath displacements in this fast-bath limit.

From Eq. (6) and the definition of $\tilde{H}_{sb}$ in Eq. (2), we obtain the population rate equation of a diagonal density-matrix element $\sigma_{\alpha\alpha}$,

$$\dot{\sigma}_{\alpha\alpha}(t) = \sum_{\xi,\eta} k_{\alpha\alpha,\xi\eta}\, \sigma_{\xi\eta}, \tag{8}$$

with α referring to a eigenstate $|\alpha\rangle$ of the renormalized exciton Hamiltonian, $\tilde{H}_s$. The eigenstate can be expressed as a

linear combination of the site excitations,

$$|\alpha\rangle = \sum_i \phi_i^\alpha |i\rangle,$$

where ϕ_i^α is the coefficient of the ith site excitation in the eigenstate $|\alpha\rangle$ ($\phi_i^\alpha = \langle i|\alpha\rangle$). We consider EET between polaronic eigenstates, which should be a physically reasonable picture for EET dynamics in the Markovian limit. Note that because the diagonalization of the renormalized Hamiltonian leads to mixing of electronic and bath degrees of freedom, the polaronic eigenstates are different from the exciton states of the undressed electronic Hamiltonian. Since the originally pure-electronic exciton should gradually mingle with motions in bath degrees of freedom during bath relaxation, when the bath reaches equilibrium, the excitation roaming on the system is no longer a bare exciton, but a polaron. Thus, treatment of EET dynamics in the Markovian limit with the polaron basis is arguably more appropriate than treatment with the undressed exciton basis. As an additional note, the small polaron transformation taken in this work generally overdresses the excitation, leading to an overly-reduced effective electronic coupling. This problem can be corrected using higher-level variational treatments that can be applied to construct polaronic zeroth-order states to better approximate the true eigenstates of the total system-plus-bath Hamiltonian.[25–28]

The population transfer rate constant from eigenstates $|\beta\rangle$ to $|\alpha\rangle$ in Eq. (8) is given as

$$\begin{aligned} k_{\alpha\alpha,\beta\beta} = \sum_{i\neq j}\sum_{m\neq n} J_{ij}J_{mn}\int_0^\infty d\tau \big\{ & \phi_i^\beta \phi_j^\alpha \phi_m^\alpha \phi_n^\beta \\ & \times e^{i(E_\beta - E_\alpha)\tau} C_{ij,mn}(\tau) \\ & + \phi_i^\alpha \phi_j^\beta \phi_m^\beta \phi_n^\alpha \times e^{-i(E_\beta - E_\alpha)\tau} C^*_{ij,mn}(\tau)\big\}, \end{aligned} \quad (9)$$

where the time-correlation function of fluctuations from system-bath coupling is

$$C_{ij,mn}(\tau) = J_{ij}J_{mn}\big[\langle\theta_i^\dagger(\tau)\theta_j(\tau)\theta_m^\dagger\theta_n\rangle - \langle\theta_i^\dagger\theta_j\rangle\langle\theta_m^\dagger\theta_n\rangle\big].$$

Equation (9) describes polaron transfer induced by fluctuations in the effective electronic couplings, which depends on the electronic coefficients that determine polaron overlap between the two states. Here the secular approximation is taken implicitly, since only population transfer dynamics is considered in Eq. (9). We define the one-sided Fourier integral of correlation functions $\tilde{C}(\omega) = \int_0^\infty e^{i\omega t}C(t)dt$, and rewrite the EET rate as

$$\begin{aligned} k_{\alpha\alpha,\beta\beta} = \sum_{i\neq j}\sum_{m\neq n} \big\{ & \phi_i^\beta \phi_j^\alpha \phi_m^\alpha \phi_n^\beta \times \tilde{C}_{ij,mn}(E_\beta - E_\alpha) \\ & + \phi_i^\alpha \phi_j^\beta \phi_m^\beta \phi_n^\alpha \times \tilde{C}^*_{ij,mn}(E_\beta - E_\alpha)\big\}. \end{aligned}$$

The correlation functions and rates can be evaluated from the spectral densities, and the results are presented in Appendix B.

C. Dimer model system

The theory presented in Subsections II A and II B is general and valid for multichromophoric systems. Nevertheless, to elucidate the physics described by the small-polaron approach, we investigate a simple model system. In this work, we consider a coupled donor-acceptor system described by the following excitonic Hamiltonian before the small-polaron transformation:

$$H_S = \begin{bmatrix} -\Delta & J_0 \\ J_0 & \Delta \end{bmatrix},$$

where 2Δ is the energy gap between the donor and the acceptor ($\Delta > 0$), and J_0 is the excitonic coupling between the two sites. We assume that the two eigenstates $|a\rangle$ and $|b\rangle$ of the renormalized Hamiltonian $\tilde{H}_s$ have eigen energies E_a and E_b, respectively, and are defined by the wavefunctions

$$\begin{aligned} |a\rangle &= \phi_1^a|1\rangle + \phi_2^a|2\rangle, \\ |b\rangle &= \phi_1^b|1\rangle + \phi_2^b|2\rangle, \end{aligned}$$

where sites 2 and 1 are the donor and acceptor, respectively. We further assume $E_b > E_a$ and consider only the downhill $|b\rangle \to |a\rangle$ EET rate in this work.

For treatment of system-bath couplings, we assume the super-Ohmic form for the spectral density,

$$\mathfrak{J}_{ij}(\omega) = \gamma_{ij}\frac{\omega^3}{\omega_c^2}e^{-\frac{\omega}{\omega_c}}, \quad (10)$$

where γ_{ij} is the electron-phonon coupling strength and ω_c is the cut-off frequency of the system-bath couplings. For this dimer model, we need to consider three spectral density functions:

$$\begin{aligned} \mathfrak{J}_{11}(\omega) &= \gamma_{11}\frac{\omega^3}{\omega_c^2}e^{-\frac{\omega}{\omega_c}}, \\ \mathfrak{J}_{22}(\omega) &= \gamma_{22}\frac{\omega^3}{\omega_c^2}e^{-\frac{\omega}{\omega_c}}, \\ \mathfrak{J}_{12}(\omega) &= \mathfrak{J}_{21}(\omega) = \gamma_{12}\frac{\omega^3}{\omega_c^2}e^{-\frac{\omega}{\omega_c}}. \end{aligned} \quad (11)$$

Note that this model is fully general with respect to the nature of the bath, and the energy fluctuations on different sites can have cross correlations. In this case, the correlated fluctuations of bath modes are described by electron-phonon coupling strength γ_{12} that is bounded by Schwarz inequality $|\gamma_{12}| \leq \sqrt{|\gamma_{11}\gamma_{22}|}$, which guarantees that the amplitude of correlated fluctuation is always smaller than that of the total fluctuations on each site. Therefore, to describe bath correlation effects, we can define a cross-correlation coefficient,

$$c = \frac{\gamma_{12}}{\sqrt{\gamma_{11}\gamma_{22}}},$$

such that $\gamma_{12} = \sqrt{\gamma_{11}\gamma_{22}} \times c$. This model then describes from fully anti-correlated baths ($c = -1$) to fully correlated baths ($c = 1$), including independent baths with $c = 0$. Thus, correlated bath effects can be accounted for within this model.

For this dimer system, the population dynamics depends on two correlation functions,

$$C_{11}(t) = J_0^2\big(\langle\theta_1^\dagger(t)\theta_2(t)\theta_1^\dagger\theta_2\rangle - \langle\theta_1^\dagger\theta_2\rangle^2\big), \quad (12)$$

$$C_{12}(t) = J_0^2\big(\langle\theta_1^\dagger(t)\theta_2(t)\theta_2^\dagger\theta_1\rangle - \langle\theta_1^\dagger\theta_2\rangle^2\big). \quad (13)$$

Following Eq. (9), the downhill EET rate from $|b\rangle$ to $|a\rangle$ can be written as

$$\begin{aligned} k_{aa,bb} &= 2[1-2(\phi_1^a\phi_1^b)^2]\times \mathrm{Re}[\tilde{C}_{12}(E_b-E_a)] \\ &\quad -4(\phi_1^a\phi_1^b)^2\times \mathrm{Re}[\tilde{C}_{11}(E_b-E_a)], \\ &\equiv k_h + k_c. \end{aligned} \tag{14}$$

Note that the factor $\phi_1^a\phi_1^b$ depends on the extent of delocalization (coherence) of the eigenstates and goes to zero when the eigenstates are fully localized (i.e., $|a\rangle = |1\rangle$ and $|b\rangle = |2\rangle$). Equation (14) shows that the EET rate is a sum of two terms. The first term (k_h) is a purely incoherent term, as it slows down when the eigenstate is more delocalized. This term resembles the Förster rate at small $\phi_1^a\phi_1^b$, i.e., weak delocalization.[33] In contrast, the second term (k_c) depends critically on the coherent delocalization of the eigenwavefunction, and is at its maximum when the eigenstate is fully delocalized. Hence, we assign k_c as the coherent term. The k_c contribution is not included in the Förster theory and therefore Eq. (14) represents an extension to the Förster theory to include contributions due to delocalization between the donor and acceptor. In Sec. III B we will investigate the dynamical behaviors of the two terms and show that they exhibit distinct temperature dependences. The small-polaron theory captures both the coherent delocalization (k_c) and incoherent hopping k_h contributions to population transfer, and thus, provides a unified perspective to the coherent effects in EET dynamics of multichromophoric systems.

III. RESULTS AND DISCUSSIONS

A. Dynamical localization

In the small-polaron theory, the electronic coupling of transformed Hamiltonian is renormalized by the factor $\langle\theta_i^\dagger\theta_j\rangle$. This term incorporates temperature dependence into the zeroth-order Hamiltonian to capture the impact of thermal fluctuations on coherence and exciton delocalization. We study the renormalization of the zeroth-order polaron Hamiltonian and its effects on the eigenstates and equilibrium structures in this section.

In Fig. 1 we show the renormalization of $\tilde{J}$ as a function of temperature at several exciton-phonon coupling strengths for the dimer model. As the temperature increases, $\langle\theta_i^\dagger\theta_j\rangle$ decays exponentially to zero. In addition, at a fixed temperature, the effective electronic coupling decreases as exciton-phonon coupling increases. Clearly, at high temperatures and strong exciton-phonon couplings, the effective coupling tends to zero. As a consequence, the transfer rate will also diminish at either of these two limits. In the small-polaron model, the renormalization of effective electronic coupling by the environmental modulations plays an important role in EET dynamics.[38]

The temperature and exciton-phonon coupling strength dependence of the effective coupling also affects the equilibrium structure of the excitonic system.[27] Figure 2 illustrates the effects of temperature as well as exciton-phonon coupling strength on the equilibrium excitonic structure for a dimer system with $\Delta = 0.1$ and $J_0 = 1$. In Fig. 2(a), we plot the off-

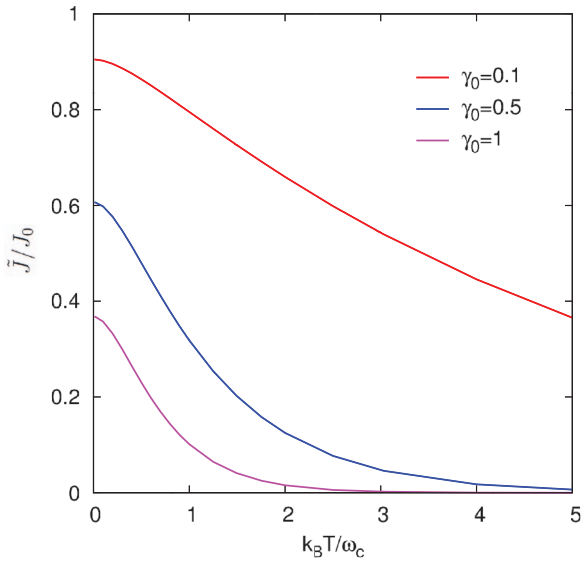

FIG. 1. Effective electronic coupling ($\tilde{J}$) as a function of temperature with exciton-phonon coupling strength $\gamma_0 = 0.1$, 0.5, and 1.0. The curves show exponential decay of effective electron couplings at high temperatures and strong exciton-phonon couplings.

diagonal element of the equilibrium reduced-system density matrix (coherence) of a model dimer system as a function of inverse temperature β and exciton-phonon coupling strength γ. As temperature increases, the coherence decreases. In addition, the increase of exciton-phonon coupling strength also lessens the coherence. To clearly show the temperature effect on the extent of delocalization for the model dimer system, we show the delocalization length, defined as the inverse participation ratio of the eigenstate,[39] as a function of β and γ in Fig. 2(b). There, as temperature increases, the delocalization length decreases and finally approaches 1. This is a result of the localization of the electronic state due to dynamical energy fluctuations induced by the bath. This dynamical localization effect is already captured in the zeroth-order description of the small-polaron theory, manifested by the renormalization of the effective electronic couplings. This is an important advantage of the polaron theory.

B. Coherent versus incoherent transfer

Let us now investigate the behavior of the rate expression in the polaron picture (Eq. (14)) under varying temperature and electron-phonon coupling strength. For simplicity, we study a model dimer system with $\Delta = 0.1\omega_c$ and $J_0 = 1\omega_c$, and assume the two sites coupled to independent baths ($c = 0$) described by the same spectral density ($\gamma_{11} = \gamma_{22} = \gamma$). Such a model is usually presumed in descriptions of EET dynamics in photosynthetic systems or organic materials.[29] Dimers with different electronic parameters show minor quantitative differences, but do not affect the general results given in this section.

In Fig. 3(a), we plot the incoherent contribution (k_h) to the downhill transfer rate (Eq. (14)) as a function of temperature and exciton-phonon coupling strength. The incoherent term shows generally thermal-activated behavior

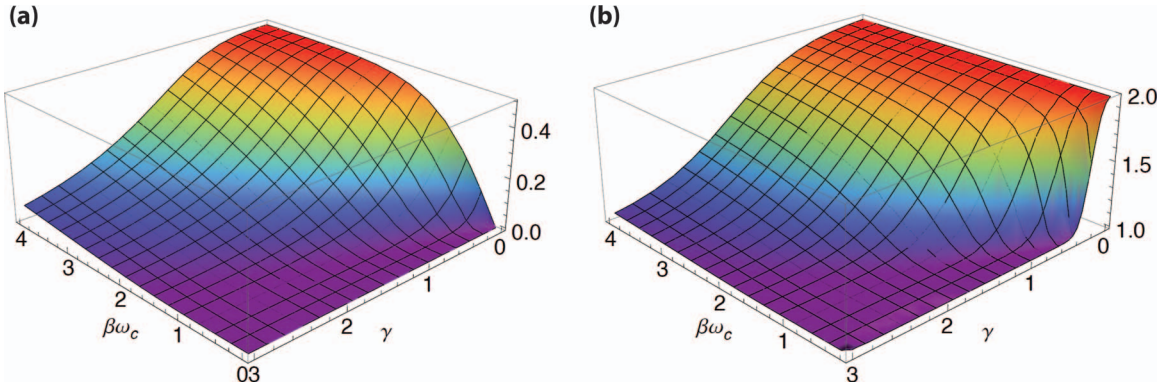

FIG. 2. Coherence and delocalization length of a two-site equilibrium density matrix as a function of inverse temperature β and exciton-phonon coupling strength γ for a model dimer system with $\Delta = 0.1$ and $J_0 = 1$. (a) Coherence (off-diagonal density matrix element) of the equilibrium state for the dimer system. (b) Delocalization length of the excitonic eigenstates of the dimer model.

that is expected from a hopping-like transfer mechanism. By contrast, the coherent term contribution (k_c) shown in Fig. 3(b) decreases as temperature increases, because as we discussed in Sec. III A, coherence is suppressed as temperature increases. As a result the coherent term only contributes to the transfer rate at low temperatures.

Figure 3(c) shows a map of the total transfer rate as a function of temperature and exciton-phonon coupling strength. This map can be viewed as a dynamical phase diagram that summarizes interesting dynamical regimes predicted by the small-polaron theory. (1) At weak exciton-phonon couplings, the EET is limited by energy dissipation to the bath, therefore, the rate is small and increases as the coupling strength γ increases. This is the general noise-assisted EET regime discussed by several other groups recently.[40–43] (2) At high temperatures and strong exciton-phonon couplings, the renormalized effective electronic coupling decays exponentially as either temperature or exciton-phonon coupling increases, which also leads to suppressed EET rate. This is a dynamical localization regime that exhibits the self-trapping of excitons.[44] (3) At intermediate coupling strengths, a regime with almost temperature-independent rate that is maximal with respect to the exciton-phonon coupling strength emerges. This optimal rate regime exists because of a subtle balance between energy dissipation and dynamical localization effects, and is also predicted by other theories.[40,41] However, the current small-polaron theory gives further insights into the mechanisms of EET through the separation of the incoherent and coherent transfer contributions. The almost temperature-independent rate is a result of a subtle balance between the coherent and incoherent contributions. At low temperatures, the EET rate is dominated by the coherent term, which decreases as temperature increases. In contrast, at high temperatures, the thermal-activated incoherent term becomes dominant. As a result, although the EET rate seems almost temperature independent in the intermediate coupling regime, the mechanism of EET exhibits a coherent to incoherent transition as temperature

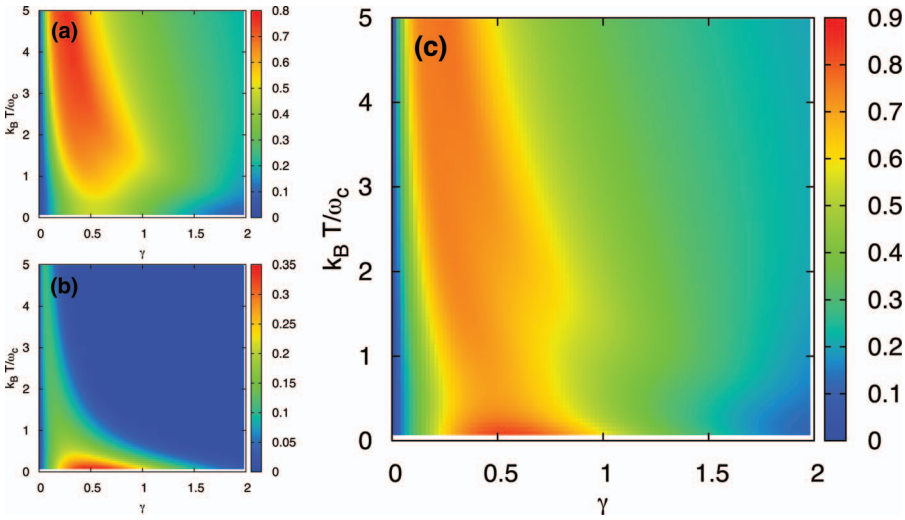

FIG. 3. Calculated downhill EET rates as a function of exciton-phonon coupling strength γ and reduced temperature k_BT/ω_c for a dimer model with $\Delta/\omega_c = 0.1$ and $J/\omega_c = 1$. In addition, here we consider uncorrelated baths and set $\gamma_{11} = \gamma_{22} = \gamma$ and $\gamma_{12} = 0$. (a) The incoherent term k_h. This term corresponds to the same hopping term in the Förster theory. (b) The coherent term k_c. This term depends on the coherence between the donor and acceptor states, and goes to zero when the eigenstate is localized. Because of the renormalization of the electronic coupling ($\tilde{J}$), the k_c term decreases as temperature increases. (c) The total rate $k_h + k_c$. Because of the interplay between the incoherent and coherent terms, the total rate exhibits a weak temperature dependence at a board temperature range in the intermediate coupling regime.

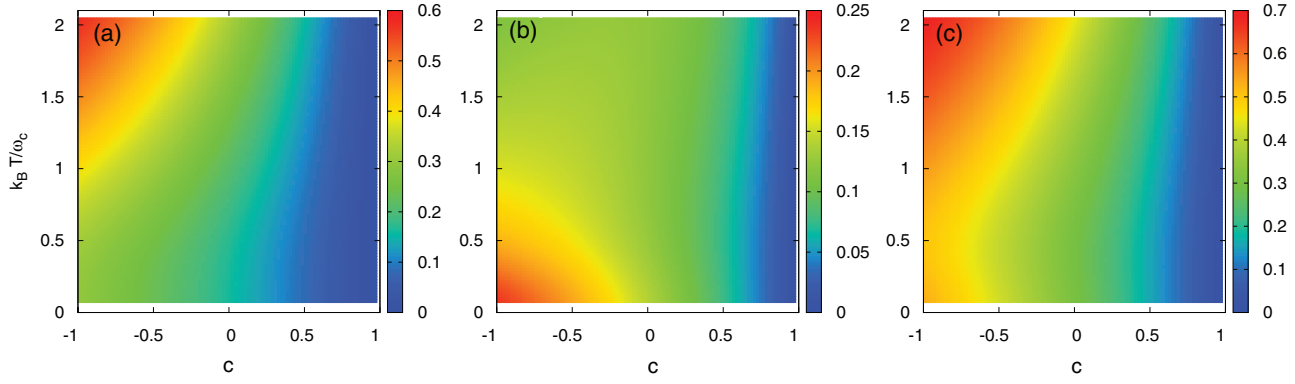

FIG. 4. Calculated downhill EET rates as a function of reduced temperature (k_BT/ω_c) and bath cross-correlation constant c for a dimer model with weak system-bath couplings ($\gamma_{11} = \gamma_{22} = 0.1$). The same electronic parameters as in Fig. 3 have been used. (a) The incoherent term k_h. (b) The coherent term k_h. (c) The total EET rate. The figure shows that fully anti-correlated bath gives the maximal EET rate. In this case, anti-correlated baths increase the amplitude of fluctuations of the energy gap between the two exciton states, leading to an increased effective system-bath coupling strength. In this weak system-bath coupling regime, an increased effective system-bath coupling strength leads to a faster rate due to noise-assisted transfer.

increases. Our results corroborated with many important theoretical findings recently, yet this theory provides intuitive physical framework to unify these discoveries.[40–42]

C. Effects of bath correlations

So far we have focused on a dimer model with uncorrelated bath, however, our theory is applicable also to correlated bath models. The nature of the protein bath modulating EET dynamics has attracted great interest recently. A coherence two-color photon-echo measurement has indicated that electronic coherence alone can not explain the long-lasting excitonic coherence observed in a bacterial photosynthetic reaction center, and a model with highly correlated bath fluctuations is required to describe the experimental data.[6] Motivated by recent experimental results, many theoretical studies have applied phenomenological models[22,43,45–47] or atomistic molecular dynamics simulations[48,49] to investigate the effect of bath correlations on the dynamics of EET. However, the influence of bath correlations on the rate of EET is still not fully elucidated, and a comprehensive understanding covering positive to negative correlations under different parameter conditions is still lacking. In this section, we investigate the EET rate for models with bath correlations and show that the polaron rate shows non-trivial bath correlation effects that yield further insights into the factors controlling the effects of bath correlations.

To elucidate the effects of bath correlations, we first calculate EET rates for a dimer model with weak exciton-phonon couplings ($\gamma_{11} = \gamma_{22} = 0.1$) at different cross correlation coefficients (Sec. II C). For simplicity, electronic parameters as in Fig. 3 have been used ($\Delta = 0.1\omega_c$ and $J_0 = 1\omega_c$). In Fig. 4, we show the calculated EET rate as a function of temperature and levels of bath correlations, from fully correlated bath ($c = 1$) to fully anti-correlated bath ($c = -1$). The EET rate exhibits strong dependence to the bath correlations. In this case, the EET rate reaches maximum when the two baths are fully anti-correlated, and gradually decreases as the cross-correlation increases. This behavior applies to both the incoherent term and the coherent term, and the temperature does not affect the position of the maximum. Here, what we have learned in Sec. III B and Eq. (A4) provides the ground rules to interpret the results. According to Eqs. (A4) and (B3), in comparison with an uncorrelated bath model, anti-correlated baths ($c < 0$) induce enhanced fluctuations in the effective couplings, while correlated baths ($c > 0$) lead to suppressed fluctuations. Because $\gamma = 0.1$ is still in the phonon-assisted transfer regime (Fig. 3(c)), increasing exciton-phonon coupling strength should lead to higher EET rate. Therefore, since anti-correlation effectively increases exciton-phonon coupling strength, as indicated in Eq. (A4), it should promote the EET rate.

In addition, we can quantify the optimal level of correlations for maximal EET rate in the dimer model by considering the exciton-phonon coupling coefficients in Eq. (A4). According to Eq. (A4), the relevant factor that contributes to the EET rate is $\Gamma_{eff} = \gamma_{ii} + \gamma_{jj} - 2\gamma_{ij}$, including the effects of bath correlations (for a independent-bath model, $\gamma_{ij} = 0$). Therefore, at the same temperature, electronic parameters, and bath cut-off frequencies, a correlated-bath model that yields maximal EET rate should have the same Γ_{eff} as an independent-bath model that also yields the maximal EET rate. As a result, we can estimate the value of optimal cross-correlation coefficient (c_{opt}) that gives rise to the maximal EET rate for a dimer system if the dynamical phase diagram (e.g., Fig. 3(c)) for the independent-bath version of the same model is known. Suppose the optimal exciton-phonon coupling strength of the independent bath model at a given temperature is γ_{opt} (i.e., the γ that gives maximal rate in Fig. 3(c)), then the c_{opt} can be approximately obtained:

$$c_{opt} = \frac{\gamma_{11} + \gamma_{22} - 2\gamma_{opt}}{2\sqrt{\gamma_{11}\gamma_{22}}}. \tag{15}$$

For the case shown in Fig. 4 at $k_BT/\omega_c \sim 1$ and $\gamma_{opt} \sim 0.5$, the estimated $c_{opt} \sim -4 > -1$. Therefore, the c_{opt} appears at the maximum anti-correlation in the dimer system described in Fig. 4.

By contrast, a dimer model with strong exciton-phonon couplings shows markedly different bath correlation effects. In Fig. 5, we show the calculated EET rate for a dimer model

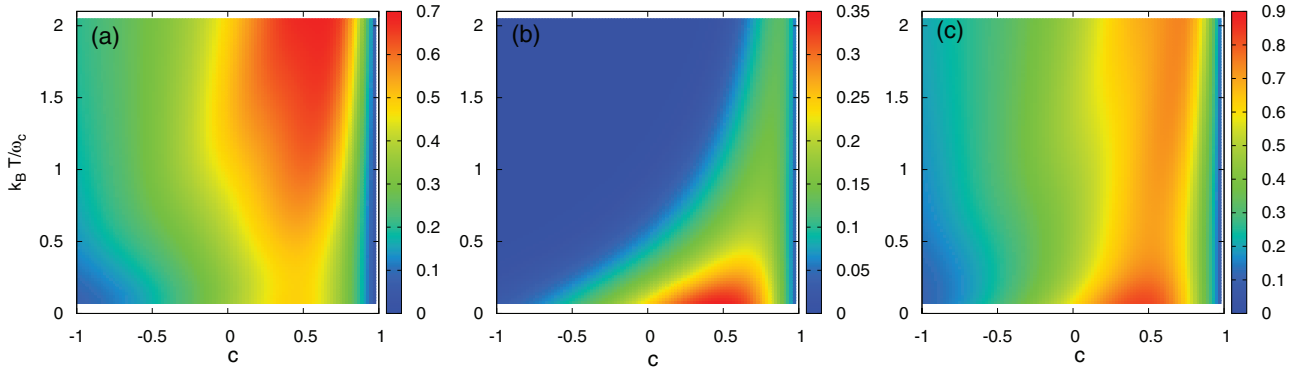

FIG. 5. Calculated downhill EET rates as a function of reduced temperature (k_BT/ω_c) and bath cross-correlation constant c for a dimer model with strong system-bath couplings ($\gamma_{11} = \gamma_{22} = 1$). The same electronic parameters as in Fig. 3 have been used. (a) The incoherent term k_h. (b) The coherent term k_h. (c) The total EET rate. The figure shows that partially correlated baths give the maximal EET rate. In this case, bath correlations reduce the amplitude of fluctuations of the energy gap between the two exciton states, leading to a reduced effective system-bath coupling strength. In this strong system-bath coupling regime, reducing effective system-bath coupling strength lessens dynamical localization, leading to a faster rate.

with strong exciton-phonon couplings ($\gamma_{11} = \gamma_{22} = 1$). The EET rate also exhibits strong dependence on the bath correlations, however, in this case the EET rate maximizes when the two baths are partially correlated ($c_{max} \sim 0.5$). This is in fact expected. According to Fig. 3(c), the dimer with $\gamma = 1$ is located in the dynamical localization regime for a uncorrelated bath model. Therefore, correlated baths, with suppressed fluctuations, could reduce dynamical localization and enhance the EET rate. An estimation based on Eq. (15) yields that at $k_BT/\omega_c \sim 1$, the c_{opt} should be about 0.5, in good agreement with the calculations presented in Fig. 5.

Although our discussions so far have focused on EET, charge transfer processes can be described within essentially the same framework. Specifically, because charge-transfer states are normally more strongly coupled to a collective bath, the current model with an anti-correlated bath ($c = -1$) is often adopted to describe charge transfer processes. Therefore, we expect the main results discussed in this work apply also to charge transfer processes. Furthermore, because in general the system-bath couplings in a charge-transfer system are stronger than those of a EET system, it is expected that the small-polaron approach should yield more accurate results for charge-transfer dynamics.

IV. CONCLUDING REMARKS

In this work, we have investigated the Markovian limit of a polaronic quantum master equation and derived a rate expression in the polaron picture to describe EET dynamics. The small-polaron EET rate contains coherent and incoherent contributions that can be easily identified. We then apply this formula to investigate EET rate for a model dimer system and reveal that the small-polaron approach predicts non-trivial temperature and exciton-phonon coupling strength dependences for the EET dynamics. When the downhill EET rate is plotted as a function of temperature and exciton-phonon coupling strength, we obtain a map of dynamical regimes that summarizes the EET rate behaviors. In addition, our results show that the interplay between the coherent contribution and the incoherent hopping contribution to the EET rate can give rise to almost temperature-independent behavior due to a coherent to incoherent transition as temperature increases.

We have also studied the bath correlation effects, and concluded that depending on the strength of system-bath couplings, the bath correlation (or anti-correlation) can either enhance or suppress EET rates. The physics is well interpreted by the interplay between noise-assisted EET and dynamical localization that we discussed in Sec. III B. An important insight is that the bath correlation effects have to be considered differently based on the strength of electron-phonon couplings. At weak system-bath couplings, anti-correlated baths promote EET because at this regime increasing effective system-bath coupling leads to higher rate. On the contrary, at strong system-bath couplings, bath correlations reduce effective fluctuations and suppress dynamical localization. As a result, correlated baths give rise to higher EET rate at strong system-bath couplings. The division of these two different behaviors is well characterized by the dynamical phase diagram as shown in Fig. 3(c) and Eq. (15).

In summary, the polaronic picture provides two useful guiding principles to describe EET rates. The first one is the principle of resonance energy transfer, which requires the donor and acceptor states to reach the same energy because of the bath-induced energy fluctuations for EET to occur. The noise-assisted energy transfer effect[40–43] is a manifestation of this principle. Effectively the noise-assisted energy transfer is described by a spectral broadening process and is captured by the spectral overlap term in the Förster theory. The second one is the dynamical localization effect that is captured by the polaronic theory. Dynamical fluctuations modify the effective electronic coupling, through a dynamical Franck-Condon factor in the polaron theory, leading to diminished transfer rate (i.e., localization) as either temperature or exciton-phonon coupling increases. Combining the two principles allows us to interpret the various dynamical regimes shown in the dynamical phase diagram (Fig. 3(c)). The same ideas apply to predict marked differences in bath correlation effects for the weak and strong exciton-phonon coupling cases. We believe the results of this work provide a useful and general perspective in the understanding of EET dynamics in molecular systems,

and will be useful to the design of efficient light-harvesting materials.

Finally we note that the polaronic quantum master equation (Eq. (5)) encapsulates additional interesting physics in EET dynamics. For example, it can be shown that the non-equilibrium phonon response to the excitation process described by the inhomogeneous terms in Eq. (5) may result in non-trivial electronic dynamics, and strong bath memory effects at strong exciton-phonon couplings. The implications of this new theoretical method in the mechanisms of ultrafast charge- and energy-transport in nanoscale molecular systems are currently under investigation and will be published in a separate work.

ACKNOWLEDGMENTS

The authors dedicate this work to the late Bob Silbey who has provided inspiration and guidance throughout this research. Y.C.C. thanks Graham Fleming and Seogjoo Jang for fruitful discussions. The financial support from the National Science Council, Taiwan (Grant No. NSC 100-2113-M-002-004-MY2), National Taiwan University (Grant No. 10R80912-5), and Center for Quantum Science and Engineering (Subproject: Grant No. 10R80914-1) are also acknowledged.

APPENDIX A: REORGANIZATION ENERGY AND THERMAL-AVERAGED FRANCK-CONDON FACTOR

The renormalized Hamiltonian in Eq. (2) depends on thermal averaged quantities including the reorganization energy and the Franck-Condon factor. Here we describe the evaluation of these quantities in terms of spectral densities that describe the system-bath couplings. Given the definition of spectral density in Eq. (4), the reorganization energy of the ith site can be written as

$$\lambda_i = \sum_n g_{ni}^2 \omega_n = \int_0^\infty \frac{\mathfrak{J}_{ii}(\omega)}{\omega} d\omega, \tag{A1}$$

and the thermal-averaged Franck-Condon factor $\langle \theta_i^\dagger \theta_j \rangle$ is

$$\begin{aligned}\langle \theta_i^\dagger \theta_j \rangle &= e^{-\frac{1}{2}\sum_n (g_{ni}-g_{nj})^2 \coth \frac{\beta\omega_n}{2}} \\ &= \exp\left\{ -\frac{1}{2}\int_0^\infty \frac{1}{\omega^2}\left[\mathfrak{J}_{ii}(\omega) - 2\mathfrak{J}_{ij}(\omega) \right.\right. \\ &\quad \left.\left. + \mathfrak{J}_{jj}(\omega)\right] \coth\frac{\beta\omega}{2} d\omega \right\}. \end{aligned} \tag{A2}$$

Note that the integral in the exponent of $\langle \theta_i^\dagger \theta_j \rangle$ diverges for Ohmic spectral densities. As a result, the current small-polaron approach does not describe electronic coherence and the transfer can only occur via the hopping mechanism for Ohmic-bath systems. This difficulty can be overcome by using a variational polaron approach.[26] For simplicity, in this work we consider exclusively a super-Ohmic form as defined in Eq. (10) to avoid this difficulty. Inserting the super-Ohmic spectral densities (Eq. (11)) into Eqs. (A1) and (A2), and performing the integrations, we obtain

$$\lambda_i = 2\gamma_{ii}\omega_c \tag{A3}$$

and

$$\begin{aligned}\langle \theta_i^\dagger \theta_j \rangle &= \exp\left[-\frac{\gamma_{ii}+\gamma_{jj}-2\gamma_{ij}}{2} \int_0^\infty d\omega \, \frac{\omega}{\omega_c^2} \right. \\ &\quad \left. \times \exp\left[-\frac{\omega}{\omega_c}\right] \coth\left(\frac{\beta\omega}{2}\right)\right] \\ &= \exp\left[-\frac{\gamma_{ii}+\gamma_{jj}-2\gamma_{ij}}{2} \left(-1 + \frac{2\psi'(\frac{1}{\beta\omega_c})}{(\beta\omega_c)^2}\right)\right], \end{aligned} \tag{A4}$$

where ψ' is the trigamma function.[50] Equation (A4) clearly shows that the γ_{ij} term gives rise to additional modulation of the effective electronic couplings due to bath correlation effects. Compared to an uncorrelated-bath model, anti-correlated baths ($c < 0$ and negative γ_{ij}) lead to enhanced fluctuations, while correlated baths ($c > 0$ and positive γ_{ij}) result in suppressed fluctuations.

APPENDIX B: EVALUATION OF TIME-CORRELATION FUNCTIONS

The dissipative dynamics in the small-polaron quantum master equation depends on the following time-correlation function:

$$C_{ij,kl}(t) = J_{ij} J_{kl} [\langle \theta_i^\dagger(t) \theta_j(t) \theta_k^\dagger \theta_l \rangle - \langle \theta_i^\dagger \theta_j \rangle \langle \theta_k^\dagger \theta_l \rangle].$$

The thermal average of the time-dependent part can be evaluated[31] to yield

$$\begin{aligned}&\langle \theta_i^\dagger(t) \theta_j(t) \theta_k^\dagger \theta_l \rangle \\ &= \langle \theta_i^\dagger \theta_j \rangle \langle \theta_k^\dagger \theta_l \rangle \exp\left[-\sum_n (g_{nj}-g_{ni})(g_{nl}-g_{nk}) \right. \\ &\quad \left. \times \cos(\omega_n t) \coth\left(\frac{\beta\omega_n}{2}\right)\right] \\ &\quad \times \exp\left[i \sum_n (g_{nj}-g_{ni})(g_{nl}-g_{nk}) \sin(\omega_n t)\right]. \end{aligned} \tag{B1}$$

Using the definition of the spectral density, the time-correlation function can be written as

$$C_{ij,kl}(t) = \tilde{J}_{ij} \tilde{J}_{kl} \{\exp[-A(t) + iB(t)] - 1\}, \tag{B2}$$

where

$$\begin{aligned} A(t) &= \int_0^\infty d\omega \, \frac{1}{\omega^2} [\mathfrak{J}_{ik}(\omega) - \mathfrak{J}_{il}(\omega) - \mathfrak{J}_{jk}(\omega) + \mathfrak{J}_{jl}(\omega)] \\ &\quad \times \cos(\omega t) \coth\left(\frac{\beta\omega}{2}\right), \\ B(t) &= \int_0^\infty d\omega \, \frac{1}{\omega^2} [\mathfrak{J}_{ik}(\omega) - \mathfrak{J}_{il}(\omega) - \mathfrak{J}_{jk}(\omega) + \mathfrak{J}_{jl}(\omega)] \sin(\omega t). \end{aligned} \tag{B3}$$

Note that we have also used the definition of the renormalized effective electronic coupling, $\tilde{J}_{ij} = J_{ij} \langle \theta_i^\dagger \theta_j \rangle$. Equation (B2)

clearly shows that the time-correlation function captures the dynamics of the *fluctuations* of the effective electronic couplings around their mean values.

Finally, assuming the super-Ohmic form for the spectral densities, the cosine integrals in Eq. (B3) can be evaluated to give

$$\begin{aligned}\int_0^\infty d\omega\, \frac{\mathfrak{J}_{ij}(\omega)}{\omega^2}\cos(\omega t)\coth\left(\frac{\beta\omega}{2}\right)&=\gamma_{ij}\int_0^\infty d\omega\, \frac{\omega}{\omega_c^2}\exp\left[-\frac{\omega}{\omega_c}\right]\cos(\omega t)\coth\left(\frac{\beta\omega}{2}\right)\\&=\gamma_{ij}\left(\frac{-1+\omega_c^2t^2}{(1+\omega_c^2t^2)^2}+\frac{2\mathrm{Re}\left[\psi'\left(\frac{1}{\beta\omega_c}+i\frac{t}{\beta}\right)\right]}{(\beta\omega_c)^2}\right),\end{aligned}\tag{B4}$$

where ψ' is the trigamma function.[50] The sine integrals in Eq. (B3) are

$$\begin{aligned}\int_0^\infty d\omega\, \frac{\mathfrak{J}_{ij}(\omega)}{\omega^2}\sin(\omega t)&=\gamma_{ij}\int_0^\infty d\omega\, \frac{\omega}{\omega_c^2}\exp\left[-\frac{\omega}{\omega_c}\right]\sin(\omega t)\\&=\gamma_{ij}\frac{2\omega_c t}{(1+\omega_c^2t^2)^2}.\end{aligned}\tag{B5}$$

[1] G. D. Scholes and G. Rumbles, Nature Mater. **5**, 683 (2006).
[2] R. E. Blankenship, *Molecular Mechanisms of Photosynthesis* (Wiley-Blackwell, 2002).
[3] R. J. Cogdell, A. T. Gardiner, H. Hashimoto, and T. H. P. Brotosudarmo, Photochem. Photobiol. Sci. **7**, 1150 (2008).
[4] Y.-C. Cheng and G. R. Fleming, Annu. Rev. Phys. Chem. **60**, 241 (2009).
[5] G. S. Engel, T. R. Calhoun, E. L. Read, T.-K. Ahn, T. Mančal, Y.-C. Cheng, R. E. Blankenship, and G. R. Fleming, Nature **446**, 782 (2007).
[6] H. Lee, Y.-C. Cheng, and G. R. Fleming, Science **316**, 1462 (2007).
[7] E. Collini and G. D. Scholes, Science **323**, 369 (2009).
[8] E. Collini, C. Y. Wong, K. E. Wilk, P. M. G. Curmi, P. Brumer, and G. D. Scholes, Nature **463**, 644 (2010).
[9] G. Panitchayangkoon, D. Hayes, K. A. Fransted, J. R. Caram, E. Harel, J. Wen, R. E. Blankenship, and G. S. Engel, Proc. Natl. Acad. Sci. U.S.A. **107**, 12766 (2010).
[10] D. Beljonne, C. Curutchet, G. D. Scholes, and R. J. Silbey, J. Phys. Chem. B **113**, 6583 (2009).
[11] R.-X. Xu and Y. Yan, Phys. Rev. E **75**, 031107 (2007).
[12] A. Ishizaki and Y. Tanimura, Chem. Phys. **347**, 185 (2008).
[13] A. Ishizaki and G. R. Fleming, J. Chem. Phys. **130**, 234111 (2009).
[14] C. Kreisbeck and T. Kramer, J. Phys. Chem. Lett. **3**, 2828 (2012).
[15] A. Ishizaki and G. R. Fleming, Proc. Natl. Acad. Sci. U.S.A. **106**, 17255 (2009).
[16] M. Sarovar, A. Ishizaki, G. R. Fleming, and K. B. Whaley, Nat. Phys. **6**, 462 (2010).
[17] C. Kreisbeck, T. Kramer, M. Rodríguez, and B. Hein, J. Chem. Theory Comput. **7**, 2166 (2011).
[18] S. Jang, Y.-C. Cheng, D. R. Reichman, and J. D. Eaves, J. Chem. Phys. **129**, 101104 (2008).
[19] S. Jang, J. Chem. Phys. **131**, 164101 (2009).
[20] S. Jang, J. Chem. Phys. **135**, 034105 (2011).
[21] A. Nazir, Phys. Rev. Lett. **103**, 146404 (2009).
[22] D. P. S. McCutcheon and A. Nazir, Phys. Rev. B **83**, 165101 (2011).
[23] A. Kolli, A. Nazir, and A. Olaya-Castro, J. Chem. Phys. **135**, 154112 (2011).
[24] R. J. Silbey and T. Harris, J. Chem. Phys. **80**, 2615 (1984).
[25] Y.-C. Cheng and R. J. Silbey, J. Chem. Phys. **128**, 114713 (2008).
[26] D. P. S. McCutcheon and A. Nazir, J. Chem. Phys. **135**, 114501 (2011).
[27] C. K. Lee, J. Moix, and J. Cao, J. Chem. Phys. **136**, 204120 (2012).
[28] E. N. Zimanyi and R. J. Silbey, Philos. Trans. R. Soc. London, Ser. A **370**, 3620 (2012).
[29] H. van Amerongen, L. Valkunas, and R. van Grondelle, *Photosynthetic Excitons* (World Scientific, 2000).
[30] T. Holstein, Ann. Phys. **8**, 343 (1959).
[31] M. Grover and R. J. Silbey, J. Chem. Phys. **54**, 4843 (1971).
[32] V. M. Kenkre and R. S. Knox, Phys. Rev. B **9**, 5279 (1974).
[33] I. I. Abram and R. Silbey, J. Chem. Phys. **63**, 2317 (1975).
[34] R. Zwanzig, Phys. Rev. **124**, 983 (1961).
[35] A. Suarez, R. J. Silbey, and I. Oppenheim, J. Chem. Phys. **97**, 5101 (1992).
[36] Y.-C. Cheng and R. J. Silbey, J. Phys. Chem. B **109**, 21399 (2005).
[37] H.-P. Breuer and F. Petruccione, *The Theory of Open Quantum Systems* (Oxford University Press, Oxford, 2002).
[38] T.-C. Yen and Y.-C. Cheng, Procedia Chem. **3**, 211 (2011).
[39] D. J. Thouless, Phys. Rep. **13**, 93 (1974).
[40] P. Rebentrost, M. Mohseni, I. Kassal, S. Lloyd, and A. Aspuru-Guzik, New J. Phys. **11**, 033003 (2009).
[41] F. Caruso, A. W. Chin, A. Datta, S. F. Huelga, and M. B. Plenio, J. Chem. Phys. **131**, 105106 (2009).
[42] J. Wu, F. Liu, Y. Shen, J. Cao, and R. J. Silbey, New J. Phys. **12**, 105012 (2010).
[43] M. Sarovar, Y.-C. Cheng, and K. B. Whaley, Phys. Rev. E **83**, 011906 (2011).
[44] Y. Toyozawa, Prog. Theor. Phys. **26**, 29 (1961).
[45] X. Chen and R. J. Silbey, J. Chem. Phys. **132**, 204503 (2010).
[46] F. Fassioli, A. Nazir, and A. Olaya-Castro, J. Phys. Chem. Lett. **1**, 2139 (2010).
[47] J. Struempfer and K. Schulten, J. Chem. Phys. **134**, 095102 (2011).
[48] C. Olbrich, J. Struempfer, K. Schulten, and U. Kleinekathoefer, J. Phys. Chem. B **115**, 758 (2011).
[49] Y. Jing, R. Zheng, H.-X. Li, and Q. Shi, J. Phys. Chem. B **116**, 1164 (2012).
[50] H. Jeffreys and B. S. Jeffreys, *Methods of Mathematical Physics*, 3rd ed. (Cambridge University Press, Cambridge, 1988), pp. 465–466.